Role of disorder in the superconducting proximity effect in *a*-$NdNi_5$/Nb bilayers

C. Cirillo,[1] A. Leo,[2] F. Urban,[2] H. Bradshaw,[3] E. Ponticorvo,[2,4] M. Sarno,[2,4] J. W. A. Robinson,[3] A. Nigro,[2] and C. Attanasio[2]

[1]*CNR-SPIN, c/o Università degli Studi di Salerno, I-84084 Fisciano (Sa), Italy*

[2]*Dipartimento di Fisica "E. R. Caianiello", Università degli Studi di Salerno, I-84084 Fisciano (Sa), Italy*

[3]*Department of Materials Science & Metallurgy, University of Cambridge, 27 Charles Babbage Road, Cambridge CB3 0FS, United Kingdom*

[4]*NANO_MATES, Research Centre for Nanomaterials and Nanotechnology at the University of Salerno, Università degli Studi di Salerno, I-84084 Fisciano (Sa), Italy*

(Received 8 October 2021; revised 29 November 2021; accepted 9 December 2021; published 22 December 2021)

The search for optimal materials to be used in superconductor/ferromagnet hybrids is fundamental to the development of superconducting spintronic devices. One of the main issues which should be tackled is the optimum ferromagnetic material that should be used in these systems, i.e., a ballistic ferromagnet with a large value of the exchange energy or a weak ferromagnet with diffusive transport. Here, we investigate the proximity effect between Nb and amorphous $NdNi_5$. We observe that the electrical transport is influenced by the strong disorder in the ferromagnetic layers. For small values of the ferromagnetic layer thickness, the depression of the superconducting critical temperature is stronger than as observed in metallic ferromagnetic layers with comparable values of the exchange energy. On the contrary, for a large thickness of the ferromagnet the interface transparency is very small and the effect of the ferromagnet on the superconductor becomes negligible. The results are in line with recent observations and confirm the prominent role played by the structural and morphological properties of the ferromagnet on the physics of superconductor/ferromagnet bilayers.

DOI: 10.1103/PhysRevB.104.214509

I. INTRODUCTION

The interplay between superconductivity and magnetism in hybrid layered structures has revealed many interesting phenomena which have been intensively studied both theoretically and experimentally for a long time now [1–3]. The superconducting properties of these structures are dictated by an unconventional proximity coupling between the superconductor (S) and the ferromagnet (F) that causes the superconducting correlations to decay with an oscillating behavior in the ferromagnetic layer [2]. The penetration of the spin-singlet Cooper pairs in the F layer is regulated by the value of the decay length ξ_{F1}, while the oscillatory length in the direction perpendicular to the interface is ξ_{F2}. One of the most relevant consequences of this property of the superconducting order parameter is the oscillation of the superconducting critical temperature (T_c) as a function of the thickness of the ferromagnetic layer (d_F) in S/F hybrids. In the dirty limit, for $E_{ex} \gg k_B T$, it is $\xi_F \equiv \xi_{F1} \simeq \xi_{F2} = \sqrt{\hbar D_F / E_{ex}}$ (D_F is the diffusion coefficient of the ferromagnet and E_{ex} is the exchange energy). For strong (weak) ferromagnets $E_{ex} \sim 1000$ (100) K and $\xi_F \sim 1$ (10) nm [4–6]. In the ballistic limit, $\xi_{F1} = \hbar v_F / 2\pi k_B T$ and $\xi_{F2} = \hbar v_F / 2E_{ex}$ (here v_F is the Fermi velocity). This implies that in clean ferromagnets singlet correlations can propagate over long distances at very low temperatures with a short oscillating length [7,8]. Therefore, the proximity effect between the S and the F layer depends not only on the strength of the magnetic order but also on the structural properties of the ferromagnet. A systematic study recently performed on $S/F/S$ junctions with Ni-based interlayers has demonstrated that strong but clean ferromagnets may be more suitable for applications in superconducting spintronics than weak but dirty ones [9].

Amorphous materials have received great attention in different areas of condensed matter physics [10,11] but their study in conjunction with superconductors has been limited to few cases [12,13]. Recently, amorphous $NdNi_5$ (hereafter *a*-$NdNi_5$) has been proposed in a thin-film form as a promising material to be used in $F/S/F$ pseudospin valve due to its narrow hysteresis loops and small exchange splitting energy [14]. However, to be concretely used in superconducting devices where the Cooper pairs can propagate over long distances in the ferromagnet, other physical quantities should be investigated. These include, as sketched above, the ferromagnetic coherence lengths and E_{ex}, but also the value of the S/F interface transparency. This property is crucial for the application of these systems in the field of superconducting spintronics [15]. A simple method to get information on these quantities is to study the transport properties of S/F bilayers, in particular the dependence of the critical temperature as a function of the S- and F-layer thicknesses. This approach, initially used for superconducting/normal metal hybrids [16–19], has been extended to the case of weak and strong ferromagnets [6,20–32], spin glasses [33,34], and a disordered antiferromagnetic alloy [35], but not to amorphous ferromagnetic materials in which the value of the correlation length (the electronic mean-free path) is smaller than the ferromagnetic coherence length.

Here, we report a study on the proximity effect in a-$NdNi_5$/Nb bilayers as a function of the thickness of both layers. The morphological characterization of the samples, in conjunction with magnetic measurements, shows the presence of Ni enriched zones in the amorphous ferromagnetic layers. The Ni segregation determines an anomalous behavior of the critical temperature of the samples when compared to results obtained in S/F bilayers containing homogeneous and metallic ferromagnets. The experimental results are influenced by an additional spin-flip scattering and are peculiar of the amorphous nature of the $NdNi_5$, which mainly determines a reduced value of the interface transparency for large $NdNi_5$ layer thickness. For small $NdNi_5$ thickness, the reduction of the critical temperature is enhanced with respect to metallic ferromagnets with similar values of E_{ex}.

II. EXPERIMENTAL AND SAMPLES CHARACTERIZATION

Sub/a-$NdNi_5$/Nb (here *Sub* stands for substrate) bilayers were deposited in an ultrahigh vacuum DC diode magnetron sputtering system on Si(100) substrates with a base pressure in the low 10^{-8} mbar range and an Ar pressure $P_{Ar}^{Nb} = 3\ \mu$bar for Nb and $P_{Ar}^{NdNi_5} = 7\ \mu$bar for $NdNi_5$. The deposition rates were 0.27 nm s^{-1} for Nb and 0.12 nm s^{-1} for $NdNi_5$, as measured by a quartz crystal monitor previously calibrated by thickness measurements made with a 3D Bruker DektakXT optical profilometer on dedicated films. Care was taken to deposit the bilayers under nominally identical conditions. More specifically, three substrates were mounted on the sample holder and, thanks to a suitable shutter positioned in the deposition chamber, it was possible to grow three bilayers which differ only for the value of the thickness of one layer in a single sputtering run. The structural, electrical, and magnetic properties of single $NdNi_5$ films have been analyzed in detail in Ref. [14]. In particular, as determined by high-resolution x-ray diffraction measurements, the films are amorphous. The electrical resistivity is about 230 $\mu\Omega$ cm, from which the electronic mean free path can be estimated to be $\ell_F \sim 0.3$ nm. Using for the Fermi velocity of the $NdNi_5$ the value $v_F = 2.94 \times 10^8$ cm/s, obtained as a weighted average of the Fermi velocities of the single elements [14,36], we obtain that the diffusion coefficient is $D_F = v_F \ell_F/3 = 2.9 \times 10^{-4}$ m^2/s. Moreover, the a-$NdNi_5$ films have a value of the low-temperature magnetization at a high field of the order of $0.3\mu_B$/atom, where μ_B is the Bohr magneton. Finally, a 10-nm-thick film has a coercive field H_c of 7 mT at $T = 5$ K.

A TESCAN-VEGA LMH-230 V microscope was used to collect scanning electron microscopy (SEM) images and analyze the morphology of the surface of a 100-nm-thick a-$NdNi_5$ film. The energy-dispersive x-ray (EDX) analyzer coupled to the microscope provided information on the chemical composition of the sample as well as the elemental distribution and concentration. Figures 1(a) and 1(b) report two SEM images taken at different resolutions, showing the morphology of the film surface. The maps of Ni and Nd, obtained by the EDX detector at low magnification, give the distribution of the two elements in the sample and an atomic ratio Ni/Nd equal to 4.8 ± 0.2, in agreement with the composition of the target used for the deposition. Moreover,

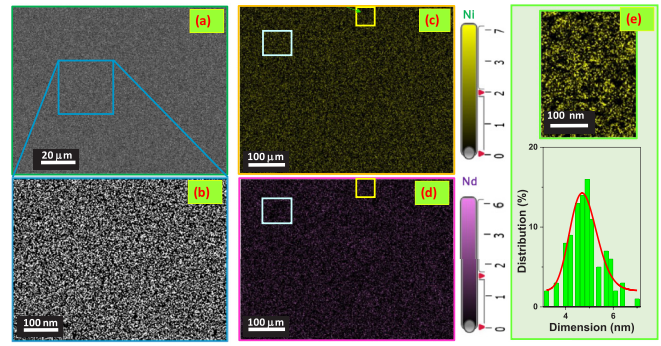

FIG. 1. (a) SEM image of the surface of a 100-nm-thick a-$NdNi_5$ film. (b) The same as in (a) but on an enlarged scale. EDX map of Ni (c) and Nd (d). (e) EDX map of Ni at higher magnification (upper panel) and size distribution histogram of the Ni clusters (lower panel). The solid line in the lower panel is a fit to the data using a log-normal distribution.

the two maps show the nonperfect superposition of the two metals distribution, as can be seen when comparing the surface areas evidenced in the yellow and light blue squares of Figs. 1(c) and 1(d). This inhomogeneity is on the length scale of few nanometers and is compatible with the presence of Ni segregation. To make a quantitative estimation of the dimensions of the Ni cluster, an EDX map of Ni has been taken at higher magnification, as shown in the upper panel of Fig. 1(e). The bidimensional image [taken on the area enclosed in the yellow box and marked by the green arrow in Fig. 1(c)] has been analyzed with the help of the software IMAGETOOL and the size of the Ni agglomerates in the investigated area has been determined. In the lower panel of Fig. 1(e) we show the histogram of the clusters' size distribution. The solid line is the fit to the data using a log-normal distribution which returns an average size of the clusters, $D = 4.9$ nm, and a variance, $\sigma = 0.6$ nm.

The presence of the Ni clusterization in the a-$NdNi_5$ films is confirmed when the temperature dependence of their saturation magnetization M_s is analyzed. Figure 2 shows the quantity $[M_{s0} - M_s(T)]/M_{s0} \equiv \Delta M_s/M_{s0}$ plotted as a function of $T^{3/2}$ and measured on a 125-nm-thick film for which $T_C = 70$ K, where T_C is Curie temperature [14]. Here M_{s0} indicates the value of M_s at $T = 5$ K. The concave curvature indicates a deviation from the $\sim T^{3/2}$ Bloch law, valid for a three-dimensional homogeneous magnetic material and due to spin-wave fluctuations [37]. In the lower inset of Fig. 2 the same data of the main panel are plotted in a log-log scale as a function of the temperature. The best fit to the data (shown by the solid line in the figure) in the high-temperature region, where ferromagnetic ordering does not coexist with a Kondo regime [14], is obtained by using the law $\Delta M_s/M_{s0} = BT^b$ with a reduced value of the exponent b, namely $b = 0.66 \pm 0.02$, and $B = (0.042 \pm 0.004)$ K$^{-0.66}$. The validity of a Bloch-type law for the saturation magnetization is common for granular magnetic materials where fluctuations of the exchange field are present [13,38]. In this case, the values of both B and b depend on the size of the magnetic grains [38]. In particular, when analyzing the magnetic behavior of iron nanoparticles very similar values for both the

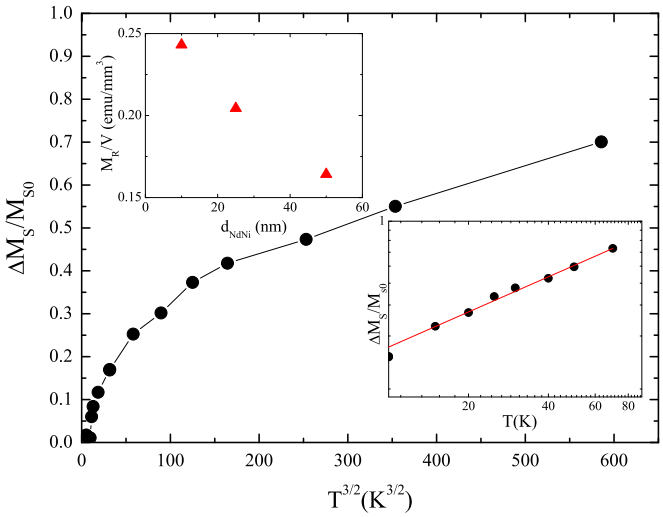

FIG. 2. Relative depression of the saturation magnetization for a 125-nm-thick a-$NdNi_5$ film as a function of $T^{3/2}$. Lower inset: the same data reported in a double logarithmic scale as a function of T. The red line is the best fit to the data (see text for details). Upper inset: d_{NdNi} dependence of the remanent magnetization per unit volume for three a-$NdNi_5$ films at 5 K.

exponent and the prefactor B have been obtained for particles with a core diameter less than 5 nm [38]. We believe that this result further supports the presence of Ni agglomerates of nanometric dimensions in the a-$NdNi_5$ films. Finally, in the upper inset of Fig. 2 the value of the remanent magnetization per unit volume at $T = 5$ K is shown for three a-$NdNi_5$ films. Again, the decreasing trend of the data could be related to the presence of the Ni clusters whose effectiveness in determining the magnetic properties of the a-$NdNi_5$ films is higher for small thickness. To close this paragraph we wish to comment on the possibility that the Ni agglomerates would behave as superparamagnetic particles since their average size D is below the superparamagnetic limit of ∼30 nm [39]. To check this possibility, we measured the temperature dependence of the magnetization in zero field cooled (ZFC) and field cooled (FC) modes using a vibrating sample magnetometer (VSM), but no clear fingerprints of a superparamagnetic behavior of the a-$NdNi_5$ films have been detected. In particular, the ZFC and FC curves do not bifurcate and the peculiar peak in the ZFC branch was not detected, maybe due to the small value of the magnetization in the films, which is close to the sensitivity of the VSM, and to a small remanent moment trapped in the superconducting magnet [14]. Nevertheless, it has been recently reported that for Ni nanoparticles of a mean diameter of 5 nm and small size distribution, the temperature at which the bifurcation (blocking temperature T_B) and the maximum in the ZFC curve appear (T_P) almost coincide and $T_B \approx T_P \approx$ 20 K [40]. Interestingly, this value is very close to the temperature where we have previously reported a change in the slope of the temperature dependence of both the coercive field and the saturation magnetization measured on a-$NdNi_5$ films. This result, also supported by electric noise spectroscopy, was interpreted as due to the presence of nanometric magnetic clusters [14].

The superconducting properties have been analyzed by electrical resistance measurements using a Cryogenic Ltd. CFM9T cryogen-free system using a standard four-probe technique on unstructured samples whose in-plane dimensions were typically 5×5 mm^2. The contacts were put in line and the distance between the current (voltage) pads was about 6 mm (1 mm). The samples were current biased with $I_b = 10$ μA. Voltage measurements have been performed in thermal electromotive force compensation mode by inverting the current direction. During the measurements, the error on the temperature value was less than 10 mK. The superconducting H-T phase diagrams were obtained by measuring the resistive transitions in the presence of the magnetic field applied parallel or perpendicular to the surface of the samples. For each field, the value of T_c was taken at the temperature where the resistance was equal to 0.5 R_N (here R_N is the normal state resistance at $T = 10$ K). The width of the resistive transitions was defined as $\Delta T_c \equiv T(R = 0.9R_N) - T(R = 0.1R_N)$. In the case of the in-plane field, this was applied perpendicularly to the direction of the bias current. To be sure that the magnetism in the a-$NdNi_5$ layers was completely saturated the following procedure was used when measuring the resistive transitions. A magnetic field of 1 T, well above H_c, was first applied to the samples at $T = 15$ K and then removed before cooling the samples down to low temperatures. When, occasionally, some $R(T)$ curves were also measured without following the above procedure no differences were observed.

Two series of Sub/a-$NdNi_5$/Nb bilayers were studied. In the first set the thickness of the a-$NdNi_5$ layer was kept constant to $d_{NdNi} = 50$ nm, while the Nb layer thickness d_{Nb} was varied between 7.5 and 60 nm. The value $d_{NdNi} = 50$ nm in the series has been chosen to be larger than the typical values obtained for the ferromagnetic coherence length in the dirty limit even for weak ferromagnets [5,6]. For comparison, a series of single Nb films was deposited to study the intrinsic effect of the T_c suppression related to the superconducting film thickness. The second set had fixed $d_{Nb} =$ 14 nm, while d_{NdNi} was varied in the range 1–100 nm. In particular, the 14-nm film has a low-temperature resistivity $\rho_S = 21$ $\mu\Omega$ cm and a superconducting critical temperature $T_{cS} = 6.74$ K. Therefore, the electronic mean-free path in Nb is $\ell_S = (\pi^2 k_B^2/v_S)/(\gamma_S \rho_S e^2) = 1.8$ nm, where $v_S = 2.73 \times 10^7$ cm/s and $\gamma_S = 7 \times 10^4$ J/K^2 cm^3 are the Fermi velocity and the electronic specific heat coefficient of Nb, respectively [41,42]. Consequently, we have for the diffusion coefficient $D_S = v_S \ell_S/3 = 1.7 \times 10^{-4}$ m^2/s and for the superconducting coherence length $\xi_S = \sqrt{\hbar D_S/2\pi k_B T_{cS}} = 5.5$ nm. Also, the ferromagnetic coherence length is $\xi_F^* = \sqrt{\hbar D_F/2\pi k_B T_{cS}} =$ 7.2 nm [43].

III. RESULTS AND DISCUSSION

In Fig. 3 the dependence of the superconducting critical temperature on d_{Nb} in a-$NdNi_5$/Nb bilayers with $d_{NdNi} =$ 50 nm is shown. The thickness dependence of T_c for a series of single Nb films with different thicknesses deposited in the same conditions of the bilayers is also reported for comparison. The results clearly show the effect of the proximity coupling in determining the suppression of T_c in the

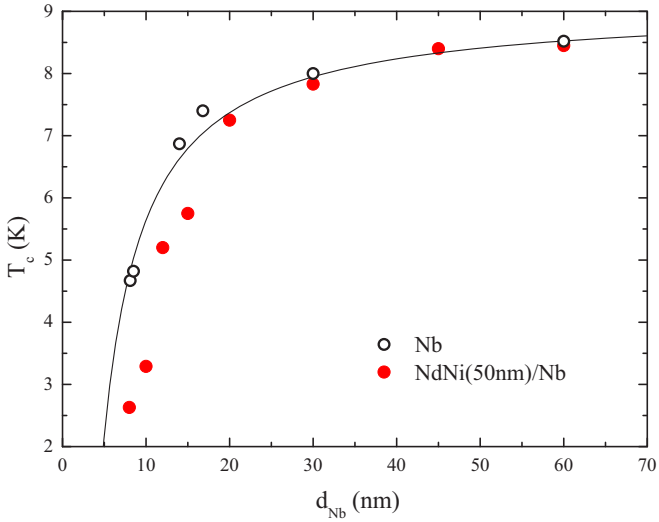

FIG. 3. T_c as a function of d_{Nb} of a-$NdNi_5$/Nb bilayers with $d_{NdNi} = 50$ nm (closed symbols). For comparison, the values of T_c for single Nb films are also reported (open symbols) together with the best fit to the data according to the Ginzburg-Landau theory (solid line).

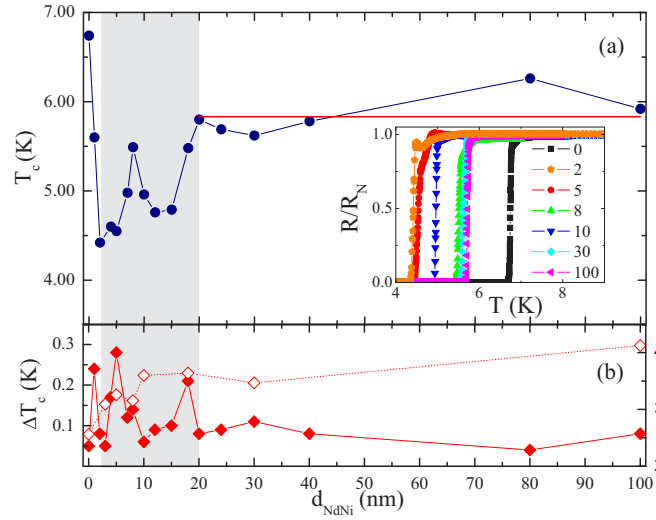

FIG. 4. (a) T_c versus d_{NdNi} of a-$NdNi_5$/Nb bilayers with $d_{Nb} = 14$ nm. The solid line is the fit to the points in the large d_{NdNi} region with the model of Ref. [43]. Inset: Resistive transitions for some bilayers of the series. (b) Left scale: Width of the resistive curves as a function of d_{NdNi} (closed symbols). Right scale: Anisotropy coefficient $\gamma = H_{c2\parallel}(0)/H_{c2\perp}(0)$ as a function of d_{NdNi} (open symbols). The grey shaded area indicates the thickness region for which the resistive transitions show a larger broadening.

bilayers with respect to the single Nb films. While the Nb data can be fitted with the formula $T_c(d_{Nb}) = T_c^{bulk}(1 - d_{crit}/d_{Nb})$ obtained in the framework of the Ginzburg-Landau theory [44] with a bulk critical temperature $T_c^{bulk} = 9.1 \pm 0.1$ K and a critical thickness $d_{crit} = 3.8 \pm 0.1$ nm (see solid line in Fig. 3), the a-$NdNi_5$/Nb data cannot be interpreted within the proximity effect theory developed for the S/F case in the dirty limit [22,43]. Despite that the data apparently show the typical increase of T_c with the thickness of the superconducting layer, any attempt to fit the data using the relevant expressions given in Ref. [43] did not succeed (in particular, in the low-thickness region), unless using unphysical values for the parameters of the theory, including an interface transparency very close to the ideal value. This, however, is not surprising since this theoretical model holds, in the dirty limit, for S/F systems containing a homogeneous ferromagnet, a condition which is not fulfilled by the a-$NdNi_5$ studied in this paper as evidenced by the structural, morphological, and magnetic characterization. Nevertheless, looking at the data the critical thickness of the Nb layer can be roughly estimated to be about 6 nm. This implies that for the a-$NdNi_5$/Nb bilayers with a thick a-$NdNi_5$ layer it is $d_{crit}/\xi_S \sim 1.1$, a number lower than the ones reported for S/F hybrids containing weak or strong nonamorphous ferromagnets [6,22,45–48].

In Fig. 4(a) the T_c versus d_{NdNi} dependence is reported. A selection of resistive transitions for some bilayers of the series is shown in the inset of the same figure. The data show a steep decrease of T_c for low d_{NdNi} values, then a region (the grey shaded area) where an unusual nonmonotonic behavior of the critical temperature is observed. Finally, a saturation value of T_c is reached for $d_{NdNi} \gtrsim 20$ nm. In the intermediate d_{NdNi} region, corresponding to the thickness range where the so-called π-state [2,49,50] takes place, along with an evident scattering of the data, we also observe a broadening of the resistive transitions, as shown in Fig. 4(b), left scale. The abrupt decrease of T_c already for $d_{NdNi} \sim 2$ nm is not expected because of the value of the magnetic moment per atom of a-$NdNi_5$ ($0.3\mu_B$/atom) which is of the same order of the magnetic moment in weak ferromagnets [51]. In fact, for S/F systems containing a weak ferromagnet the minimum in the T_c versus d_F curve (d_F is the thickness of the F layer) is for $d_F \sim 4$ nm [6,45] while the minimum at $d_F \sim 2$ nm has been observed in Nb/Ni bilayers [52,53]. We believe that this behavior is related to the additional spin-flip scattering which plays a relevant role when a strongly inhomogeneous ferromagnet is considered in the S/F theory [13,54]. On the contrary, for thick enough $NbNi_5$ layers the magnetic disorder reduces the value of the interface transparency and this results in a smaller decrease of the critical temperature with respect to the homogeneous case [13,54]. This explains the fact that T_c saturates at about 6 K, a value comparable with T_{cS}. Furthermore, the ratio of T_c at large d_{NdNi} and the lowest measured value at about $d_{NdNi} \sim 5$ nm is 1.25. This number is always much smaller and typically of the order of the unity for S/F bilayers containing a metallic ferromagnet [6,25,52,53]. The reduction of the interface transparency for thick $NbNi_5$ layers is also responsible of the observed small value of d_{crit}. However, the model developed in Ref. [43] can be used to roughly reproduce the values of the critical temperatures in the region of large d_{NdNi} where T_c saturates. The parameter which in the theory describes the effect of the interface transparency, $\mathcal{T}$, is $\gamma_b = [2\ell_F(1 - \mathcal{T})]/(3\xi_F^*\mathcal{T})$. Since both ℓ_F and ξ_F have been already evaluated independently, $\mathcal{T}$ is left as the only free parameter. A nice agreement with the experimental data is obtained for $\mathcal{T} \approx 0.08$ [solid line in Fig. 4(a)]. This value is indeed much lower than those estimated for well-known S/F systems obtained with weak ferromagnets [26]. Finally,

we wish also to comment on the trend of T_c and ΔT_c for 3 nm $\lesssim d_{NdNi} \lesssim$ 20 nm, where critical temperature data are strongly scattered and the width of the resistive transitions relatively large. We believe that this behavior could be related to the Ni clusterization in the a-$NdNi_5$ layers, which determines a distribution of the exchange energy within the ferromagnetic layer. As shown in the case of Nb/CuNi hybrids, the presence of magnetic inhomogeneities may be responsible for the broadening of the resistive transitions [51]. Moreover, the noisy T_c behavior can be ascribed to the nonmonotonic behavior of ξ_{F1} and ξ_{F2} in the presence of the Ni inclusions [8], since they can hardly be linked to fluctuations of the magnetic properties of the a-$NdNi_5$ layers (see the upper inset of Fig. 2). It is reasonable to expect that these effects are more pronounced when d_{NdNi} is comparable to the size of the Ni clusters. However, even in the presence of scattered data in the T_c versus d_{NdNi} curve plotted in Fig. 4 we can roughly estimate the value of E_{ex} for the a-$NdNi_5$. Due to the extremely reduced value of $\ell_F \sim 0.3$ nm, we can safely assume that it is smaller than all the characteristic lengths of the problem so that the ferromagnet is in the dirty limit. In this regime, ξ_F, it is related to the position of the minimum in the T_c versus d_{NdNi} curve [Fig. 4(a)] through the relation $d_{min} = 0.7\pi\xi_F/2$ [43]. Therefore, from d_{min} the value of the exchange energy, $E_{ex} = (0.35\pi)^2\hbar D_F/d_{min}^2$, can be determined. In our case, taking $d_{min} \sim 2$ nm in correspondence of the first local minimum in the curve, we obtain $E_{ex} \sim 430$ K, which is consistently almost one order of magnitude smaller than the value reported for elemental Ni [55] and of the same order of the exchange energy reported for crystalline $NdNi_5$ [56].

In the Figs. 5(a) and 5(b) are shown, respectively, the resistive transition curves measured in the presence of a parallel and perpendicular magnetic field for the bilayer of the series with variable d_{NdNi} having $d_{NdNi} = 5$ nm. The corresponding curve measured in zero field and plotted in the inset of Fig. 4(a), shows a two-step transition at the onset of the $R(T)$ curve which tends to disappear when the magnetic field is increased. This evidence rules out the possibility that the broadening of the resistive curves is related to sample inhomogeneities which give rise to regions with different superconducting critical temperatures [57]. On the contrary, the curves of the sample of the same series with $d_{NdNi} = 30$ nm [Figs. 5(c) and 5(d)] have narrower transition widths, almost independent on H. These results are summarized in Fig. 5(e) where the magnetic field dependence of ΔT_c is reported. Open and closed circles refer to the sample with $d_{NdNi} = 5$ nm in the perpendicular and parallel configuration of the magnetic field, respectively. Green triangles represent the field dependence of the transition widths for the bilayer with $d_{NdNi} = 30$ nm in the parallel configuration (similar results are obtained in the perpendicular case). A very similar result has been obtained in the case of $S/F/S$ trilayers for thicknesses of the ferromagnetic layer where the π phase [2,49,50,58] could be expected. This experimental evidence was related to the occurrence of a Josephson-like coupling between the superconducting layers which is suppressed at high magnetic fields [57]. In this thickness region the resistive transitions of the $S/F/S$ trilayers show a larger broadening. The model proposed in Ref. [57] can be also applied to the case of S/F bilayers under study

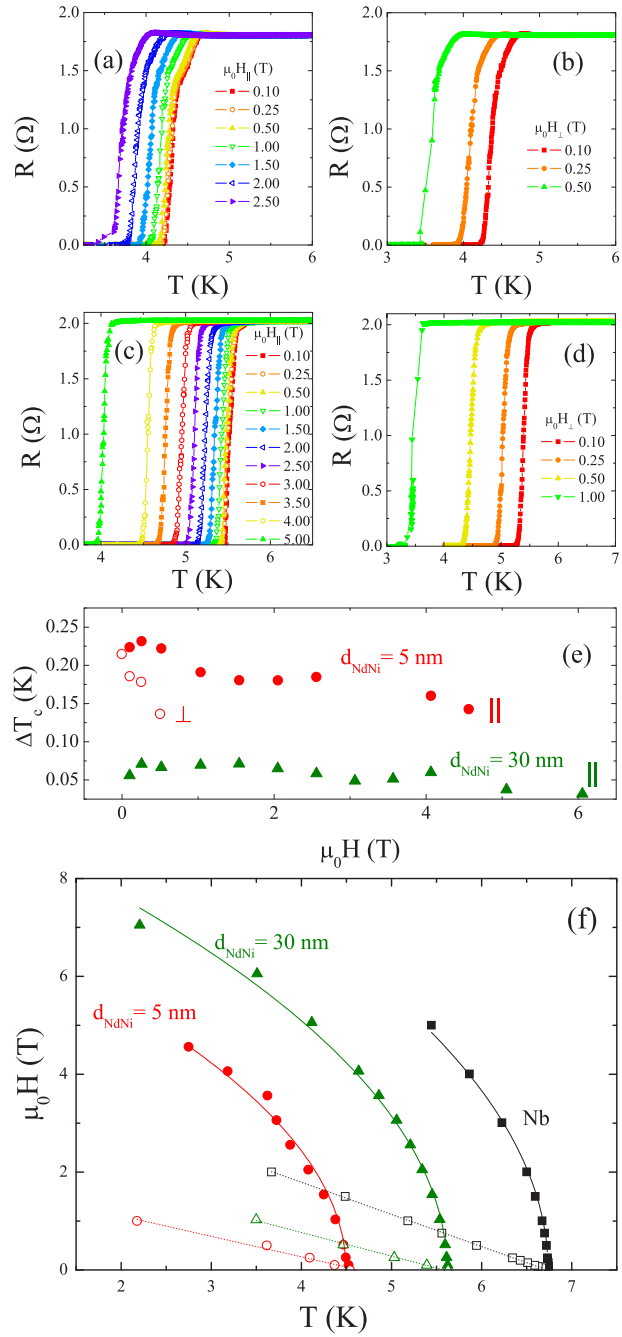

FIG. 5. (a) [(b)] Selection of resistive transitions of the a-$NdNi_5$/Nb bilayer with $d_{NdNi} = 5$ nm in the presence of a parallel (perpendicular) magnetic field, whose values are reported in the graphs. (c) [(d)] Selection of resistive transitions of the a-$NdNi_5$/Nb bilayer with $d_{NdNi} = 30$ nm in the presence of a parallel (perpendicular) magnetic field, whose values are reported in the graphs. (e) Dependence of the width of the resistive transitions of the a-$NdNi_5$/Nb bilayer with $d_{NdNi} = 5$ nm in perpendicular (open circles) and parallel (closed circles) magnetic field. The closed triangles show ΔT_c versus the parallel magnetic magnetic field of the a-$NdNi_5$/Nb bilayer with $d_{NdNi} = 30$ nm. (f) Parallel (closed symbols) and perpendicular (open symbols) superconducting phase diagram of a 14-nm-thick single Nb film (black squares) and two bilayers of the series with variable d_{NdNi}: $d_{NdNi} = 30$ nm (green triangles) and $d_{NdNi} = 5$ nm (red circles). The solid and the broken lines are the best fit to the data (see text for details).

at the first stages of the superconducting transition, when the S layer consists of both superconducting and normal island, coupled out-of-plane via the F layer, which, in turn, consists of regions with different magnetic strength. We believe that this observation is again related to the presence of the Ni clusters whose dimensions, looking at the grey shaded area in Fig. 4, should be definitely smaller than 20 nm since the bilayers with d_{NdNi} out of this thickness range show sharp transitions. Finally, the Ni segregation does not have any effect on the phase diagram of the a-$NdNi_5$/Nb bilayers. In Fig. 5(f) is shown the temperature behavior of the perpendicular, $H_{c2\perp}$, and of the parallel, $H_{c2\parallel}$, critical magnetic fields of the two bilayers with $d_{\mathrm{NdNi}} = 5$ and 30 nm. For comparison, in the same figure the phase diagram of a 14-nm-thick Nb single film is also reported. The solid lines in panel (f) of the figure are the best fit to the $H_{c2\parallel}(T)$ data for the three samples using the relation $H_{c2\parallel}(T) = H_{c2\parallel}(0)(1 - T/T_c)^{1/2}$, valid for a two-dimensional (2D) [59] superconductor, leaving $H_{c2\parallel}(0)$ as the only free parameter. The nice agreement with the experimental data in the entire temperature range witnesses of a 2D behavior also very close to T_c. The broken lines in the same figure reproduce the linear best fit to the $H_{c2\perp}(T) = H_{c2\perp}(0)(1 - T/T_c)$ data [59]. From $H_{c2\perp}(0)$ the Ginzburg-Landau coherence length can be calculated using the relation $\xi_{GL} = [\Phi_0/2\pi H_{c2\perp}(0)]^{1/2}$ [59]. In the case of the single Nb film, we have $\xi_S = (2/\pi)\xi_{GL} \sim 5.5$ nm, in good agreement with the result obtained above when considering the diffusion coefficient of Nb. From the zero-temperature values of the parallel and perpendicular magnetic field it is possible to estimate the anisotropy coefficient $\gamma = H_{c2\parallel}(0)/H_{c2\perp}(0)$ [60]. As shown in the right scale of Fig. 4(b), its monotonous increase up to a saturation value obtained already for $d_{\mathrm{NdNi}} \sim 10$ nm indicates a progressive diminution of the effective Nb thickness due to the influence of the increasing value of d_{NdNi} [60].

IV. CONCLUSIONS

In summary, we have reported compositional, magnetic, and superconducting properties of a-$NdNi_5$/Nb bilayers. The behaviors of the superconducting critical temperature as a function of both d_{Nb} and d_{NdNi} are strongly determined by the inhomogeneous magnetic nature of the amorphous ferromagnetic layer and they cannot be described by the proximity theory developed in the dirty limit for homogeneous metallic ferromagnets. Our results are in qualitative agreement with the theory developed in the case of a ferromagnet in which a spin-scattering mechanism plays a relevant role [54]. The experimental data show that amorphous materials, despite their relatively low value of exchange energy, are not suitable in superconducting spintronic because of the strongly diffusive transport of the Cooper pairs and the very small S/F interface transparency for large a-$NdNi_5$ layer thickness. The results are consistent with recent experiments performed in $S/F/S$ junctions containing Ni-based ferromagnetic interlayers where it has been shown that strong-but-clean ferromagnets are more suitable in superconducting spintronics than weak-but-dirty ferromagnetic alloys [9].

ACKNOWLEDGMENTS

The authors acknowledge M. Yu. Kupriyanov for useful suggestions and the careful reading of the manuscript. This research was partially supported by the Italian National Operative Programme for Research and Competitiveness 2007-2013, funded by the European Union.

[1] A. A. Golubov, M. Yu. Kupriyanov, and E. Il'ichev, Rev. Mod. Phys. **76**, 411 (2004).
[2] A. I. Buzdin, Rev. Mod. Phys. **77**, 935 (2005).
[3] M. G. Blamire and J. W. A. Robinson, J. Phys.: Condens. Matter **26**, 453201 (2014).
[4] J. W. A. Robinson, S. Piano, G. Burnell, C. Bell, and M. G. Blamire, Phys. Rev. Lett. **97**, 177003 (2006).
[5] V. V. Ryazanov, V. A. Oboznov, A. Yu. Rusanov, A. V. Veretennikov, A. A. Golubov, and J. Aarts, Phys. Rev. Lett. **86**, 2427 (2001).
[6] C. Cirillo, S. L. Prischepa, M. Salvato, C. Attanasio, M. Hesselberth, and J. Aarts, Phys. Rev. B **72**, 144511 (2005).
[7] F. Konschelle, J. Cayssol, and A. Buzdin, Phys. Rev. B **82**, 180509(R) (2010).
[8] N. G. Pugach, M. Yu. Kupriyanov, E. Goldobin, R. Kleiner, and D. Koelle, Phys. Rev. B **84**, 144513 (2011).
[9] O. M. Kapran, T. Golod, A. Iovan, A. S. Sidorenko, A. A. Golubov, and V. M. Krasnov, Phys. Rev. B **103**, 094509 (2021).
[10] R. Streubel, C.-H. Lambert, N. Kent, P. Ercius, A. T. N'Diaye, C. Ophus, S. Salahuddin, and P. Fischer, Adv. Mater. **30**, 1800199 (2018).
[11] N. Chen, K. Fang, H. Zhang, Y. Zhang, W. Liu, K. Yao, and Z. Zhang, J. Semicond. **40**, 081510 (2019).
[12] C. Bell, S. Turşucu, and J. Aarts, Phys. Rev. B **74**, 214520 (2006).
[13] A. Alija, D. Pérez de Lara, E. M. Gonzalez, G. N. Kakazei, J. B. Sousa, J. P. Araujo, A. Hierro-Rodriguez, J. I. Martín, J. M. Alameda, M. Vélez, and J. L. Vicent, Phys. Rev. B **82**, 184529 (2010).
[14] C. Cirillo, C. Barone, H. Bradshaw, F. Urban, A. Di Bernardo, C. Mauro, J. W. A. Robinson, S. Pagano, and C. Attanasio, Sci. Rep. **10**, 13693 (2020).
[15] J. Linder and J. W. A. Robinson, Nat. Phys. **11**, 307 (2015).
[16] A. A. Golubov, Proc. SPIE **2157**, 353 (1994).
[17] C. Cirillo, S. L. Prischepa, M. Salvato, and C. Attanasio, Eur. Phys. J. B **38**, 59 (2004).
[18] A. Tesauro, A. Aurigemma, C. Cirillo, S. L. Prischepa, M. Salvato, and C. Attanasio, Supercond. Sci. Technol. **18**, 1 (2005).
[19] V. N. Kushnir, S. L. Prischepa, C. Cirillo, and C. Attanasio, J. Appl. Phys. **106**, 113917 (2009).
[20] J. S. Jiang, D. Davidović, D. H. Reich, and C. L. Chien, Phys. Rev. Lett. **74**, 314 (1995).

[21] J. S. Jiang, D. Davidović, D. H. Reich, and C. L. Chien, Phys. Rev. B **54**, 6119 (1996).

[22] J. Aarts, J. M. E. Geers, E. Brück, A. A. Golubov, and R. Coehoorn, Phys. Rev. B **56**, 2779 (1997).

[23] A. Potenza and C. H. Marrows, Phys. Rev. B **71**, 180503(R) (2005).

[24] V. Zdravkov, A. Sidorenko, G. Obermeier, S. Gsell, M. Schreck, C. Müller, S. Horn, R. Tidecks, and L. R. Tagirov, Phys. Rev. Lett. **97**, 057004 (2006).

[25] C. Cirillo, A. Rusanov, C. Bell, and J. Aarts, Phys. Rev. B **75**, 174510 (2007).

[26] J. Aarts, C. Attanasio, C. Bell, C. Cirillo, M. Flokstra, and J. M. van der Knaap, Superconductor/ferromagnet hybrids: Bilayers and spin switching, in *Nanoscience and Engineering in Superconductivity*, Nanoscience and Technology series, edited by V. Moshchalkov, R. Wördenweber, and W. Lang, (Springer, Berlin, 2010), pp. 323–347.

[27] V. I. Zdravkov, J. Kehrle, G. Obermeier, S. Gsell, M. Schreck, C. Müller, H.-A. Krug von Nidda, J. Lindner, J. Moosburger-Will, E. Nold, R. Morari, V. V. Ryazanov, A. S. Sidorenko, S. Horn, R. Tidecks, and L. R. Tagirov, Phys. Rev. B **82**, 054517 (2010).

[28] D. Mancusi, E. A. Ilyina, V. N. Kushnir, S. L. Prischepa, C. Cirillo, and C. Attanasio, J. Appl. Phys. **110**, 113904 (2011).

[29] Yu. Khaydukov, R. Morari, O. Soltwedel, T. Keller, G. Christiani, G. Logvenov, M. Kupriyanov, A. Sidorenko, and B. Keimer, J. Appl. Phys. **118**, 213905 (2015).

[30] Yu. N. Khaydukov, A. S. Vasenko, E. A. Kravtsov, V. V. Progliado, V. D. Zhaketov, A. Csik, Yu. V. Nikitenko, A. V. Petrenko, T. Keller, A. A. Golubov, M. Yu. Kupriyanov, V. V. Ustinov, V. L. Aksenov, and B. Keimer, Phys. Rev. B **97**, 144511 (2018).

[31] W. M. Mohammed, I. V. Yanilkin, A. I. Gumarov, A. G. Kiiamov, R. V. Yusupov, and L. R. Tagirov, Beilstein J. Nanotechnol. **11**, 807 (2020).

[32] I. Yanilkin, W. Mohammed, A. Gumarov, A. Kiiamov, R. Yusupov, and L. Tagirov, Nanomaterials **11**, 64 (2021).

[33] L. V. Mercaldo, C. Attanasio, C. Coccorese, L. Maritato, S. L. Prischepa, and M. Salvato, Phys. Rev. B **53**, 14040 (1996).

[34] C. Attanasio, C. Coccorese, L. V. Mercaldo, S. L. Prischepa, M. Salvato, and L. Maritato, Phys. Rev. B **57**, 14411 (1998).

[35] C. Bell, E. J. Tarte, G. Burnell, C. W. Leung, D.-J. Kang, and M. G. Blamire, Phys. Rev. B **68**, 144517 (2003).

[36] N. W. Ashcroft and D. N. Mermin, *Solid State Physics* (Saunders College, Philadelphia, 1976).

[37] R. C. O'Handley, *Modern Magnetic Materials: Principles and Applications* (Wiley, New York, 1999).

[38] D. Zhang, K. J. Klabunde, C. M. Sorensen, and G. C. Hadjipanayis, Phys. Rev. B **58**, 14167 (1998).

[39] K. M. Krishnan, IEEE Trans. Mag. **46**, 2523 (2010).

[40] J. T. Batley, M. Nguyen, I. Kamboj, C. Korostynski, E. S. Aydil, and C. Leighton, Chem. Mater. **32**, 6494 (2020).

[41] H. R. Kerchner, D. K. Christen, and S. T. Sekula, Phys. Rev. B **24**, 1200 (1981).

[42] *Handbook of Chemistry and Physics*, edited by R. C. Weast (The Chemical Rubber Co. Cleveland, 1972).

[43] Ya. V. Fominov, N. M. Chtchelkatchev, and A. A. Golubov, Phys. Rev. B **66**, 014507 (2002).

[44] J. Simonin, Phys. Rev. B **33**, 7830 (1986).

[45] A. Rusanov, R. Boogaard, M. Hesselberth, H. Sellier, and J. Aarts, Phys. C (Amsterdam, Neth.) **369**, 300 (2002).

[46] C. Strunk, C. Sürgers, U. Paschen, and H. v. Löhneysen, Phys. Rev. B **49**, 4053 (1994).

[47] Th. Mühge, K. Westerholt, H. Zabel, N. N. Garif'yanov, Yu. V. Goryunov, I. A. Garifullin, and G. G. Khaliullin, Phys. Rev. B **55**, 8945 (1997).

[48] L. Lazar, K. Westerholt, H. Zabel, L. R. Tagirov, Yu. V. Goryunov, N. N. Garif'yanov, and I. A. Garifullin, Phys. Rev. B **61**, 3711 (2000).

[49] Z. Radović, L. Dobrosavljević-Grujić, A. I. Buzdin, and J. R. Clem, Phys. Rev. B **38**, 2388 (1988).

[50] A. I. Buzdin and M. Yu. Kupriyanov, Pis'ma v Zh. Eksp. Teor. Fiz. **52**, 1089 (1990) [Sov. Phys. JETP Lett. **52**, 487 (1990)].

[51] V. N. Kushnir, S. L. Prischepa, J. Aarts, C. Bell, C. Cirillo, and C. Attanasio, Eur. Phys. J. B **80**, 445 (2011).

[52] A. S. Sidorenko, V. I. Zdravkov, A. A. Prepelitsa, C. Helbig, Y. Luo, S. Gsell, M. Schreck, S. Klimm, S. Horn, L. R. Tagirov, and R. Tidecks, Ann. Phys. **12**, 37 (2003).

[53] T. R. Lemberger, I. Hetel, A. J. Hauser, and F. Y. Yang, J. Appl. Phys. **103**, 07C701 (2008).

[54] M. Fauré, A. I. Buzdin, A. A. Golubov, and M. Yu. Kupriyanov, Phys. Rev. B **73**, 064505 (2006).

[55] V. Shelukhin, A. Tsukernik, M. Karpovski, Y. Blum, K. B. Efetov, A. F. Volkov, T. Champel, M. Eschrig, T. Löfwander, G. Schön, and A. Palevski, Phys. Rev. B **73**, 174506 (2006).

[56] R. J. Radwański and N. H. Kim-Ngan, J. Alloys Compd. **219**, 260 (1995).

[57] S. L. Prischepa, C. Cirillo, C. Bell, V. N. Kushnir, J. Aarts, C. Attanasio, and M. Yu. Kupriyanov, JETP Lett. **88**, 375 (2008).

[58] Z. Radović, M. Ledvij, L. Dobrosavljević-Grujić, A. I. Buzdin, and J. R. Clem, Phys. Rev. B **44**, 759 (1991).

[59] M. Tinkham, *Introduction to Superconductivity* (Mc Graw-Hill, New York, 1975).

[60] C. Cirillo, C. Bell, G. Iannone, S. L. Prischepa, J. Aarts, and C. Attanasio, Phys. Rev. B **80**, 094510 (2009).